A case for possible late glaciofluvial activity on Eastern Hellas basin: Valley morphologies and glacial signatures.

E. Blanc[1] *(evan.blanc@etu.univ-nantes.fr)*, **A. Grau Galofre**[1], **N. Mangold**[1], **S. Berquez**[1], **N. Le Becq**[1]
[1]*Laboratoire de Planétologie et Géosciences, Nantes Universtié, Univ. Angers, Le Mans Université, CNRS UMR 6112, France.*

Introduction:

During episodes of high obliquity, the martian mid-latitudes acted as a cold trap and saw the enhanced deposition of ice and the development of ice masses[1,2], whereas ice deposition focused on the polar regions at moderate and low obliquity scenarios. Within the mid-latitudes, the Hellas Basin, with its unique topography, had an important effect on the distribution of moisture and water vapor, leading to enhanced ice accumulation on the eastern side of the basin rim[1,2]. In turn, this climate led to the development of significant ice masses, either in the form of widespread viscous flow features (VFF)[3] or possibly as a large ice sheet, which would have flown downwards into the Hellas basin[4].

The study area (Fig. 1) is located along the eastern rim of the Hellas Basin, a region shaped by various geological processes, including volcanic activity (Tyrrhena Patera, Hadriaca Patera), fluvial erosion (Reull Vallis, Teviot Vallis), and more recent deposition of an ice-rich mantle known as the Latitude Dependent Mantle (LDM)[5]. On the plateau west of Reull Vallis, near the Apece Crater (Fig. 1), numerous fresh and well-preserved valley networks, extending over several hundred kilometers, are found on terrains identified as Hesperian and Noachian highlands[6]. These networks generally follow an east-west orientation, consistent with the regional slope that gently sloping downward the center of Hellas.

By observing the different landforms of the area, we are working to build a global understanding of regional geology. The observations include the present-day morphologies mapping and their interactions. Then, we will propose in-depth analysis of valley system dynamics. Through hypothesis regarding the formation conditions of this valleys network, we will replace the climatic context of the region over time.

Methods:

We worked to produce an initial mapping of the landforms presents in the study area with ArcGIS software, using basemaps image data from the Mosaic Tiles by Murray Lab V01, which integrates Con-

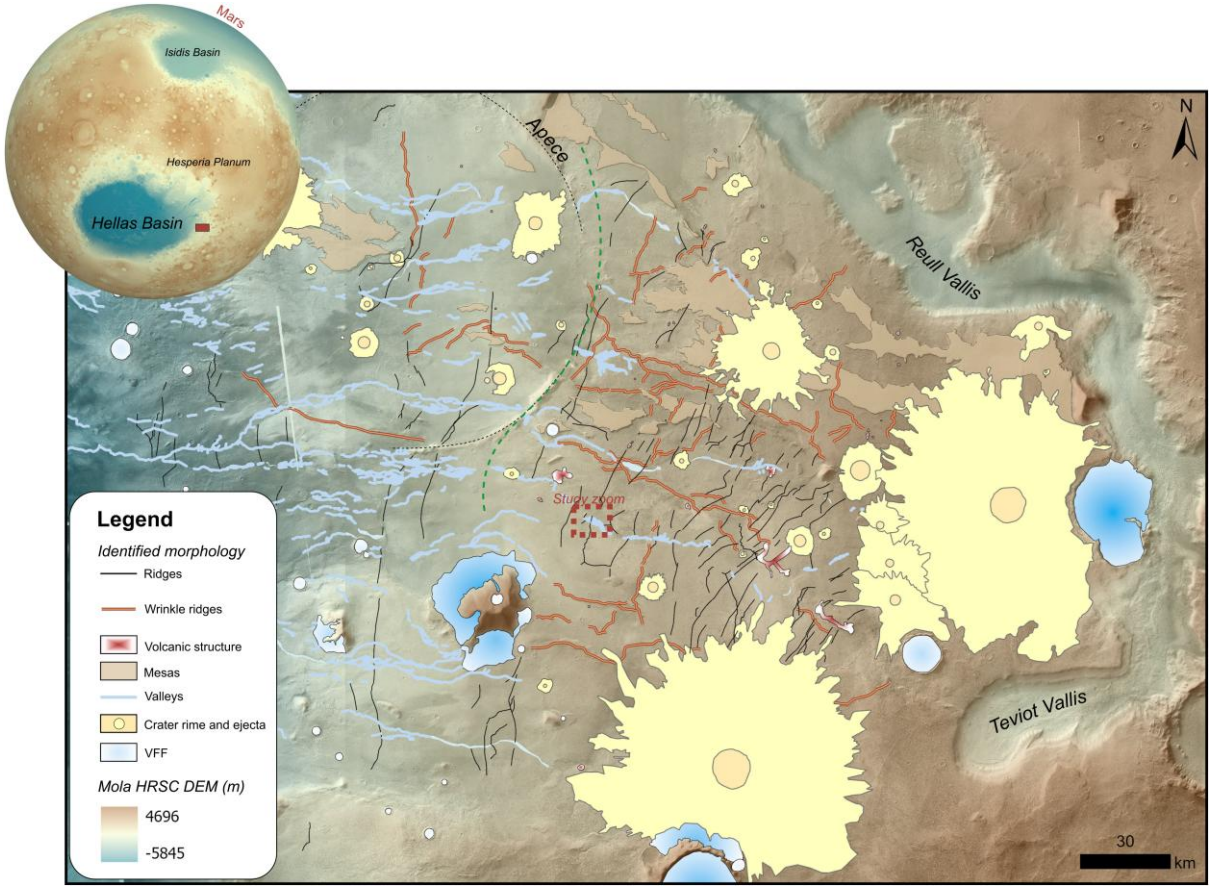

Figure 1: Geomorphologic map of the study area. The green dotted line marks is the transition in valley morphology, and the red dotted square highlights the detailed study area.

text Camera (CTX) data at 6 m/pixel resolution[7,8].

We perfomed manual mapping of the different valleys present in the region of interest, by drawing a polyline along the main valley axis. While the CTX mosaic was the primary dataset used to identify these systems, it was in some cases necessary to use individual tiles with the JMARS online GIS platform[9], as they occasionally offer better quality depending on lighting conditions or image artifacts.

Some landforms, such as mesas, covering mainly the north of the study area (Fig.1), were identified by their elevation of around 200m above the basal unit, and are characterized by relatively flat tops and steep sides. For more complex landforms, identification was supported by previous literature. This is the case with wrinkle ridges, commonly defined as asymmetrical ridges, typically composed of a broad linear rise with complex crenulations, occurring on broad, low-relief[10,11].

We use the generic term ridges to describe linear positive relief features, ranging from a few tens to several hundreds of meters in width, and mapped as black lines (Fig. 1). These features are approximatively parallel, extend over distances from a few kilometers to several hundred kilometers, and often appear perpendicular to the valleys. Some studies suggest that, based on their length/continuity and surface expression, certain ridges may correspond to dyke systems[12]. However, many of these ridges have morphologies that are inconsistent with dyke systems, such as arcuate shapes or discontinuous cross-sections. Therefore, we have chosen not to assign a definitive classification at this stage.

In addition, volcanic structures are present upstream of the valleys (Fig. 1). These features generally appear as domes or mounds, though some propose more complex and elongated shapes. Based on comparisons with similar landforms observed elsewhere on Mars, they are likely associated with volcanic intrusions or volcanic domes[13,14]. These observations were supplemented with data from THEMIS Nighttime, a thermal infrared system, with a surface

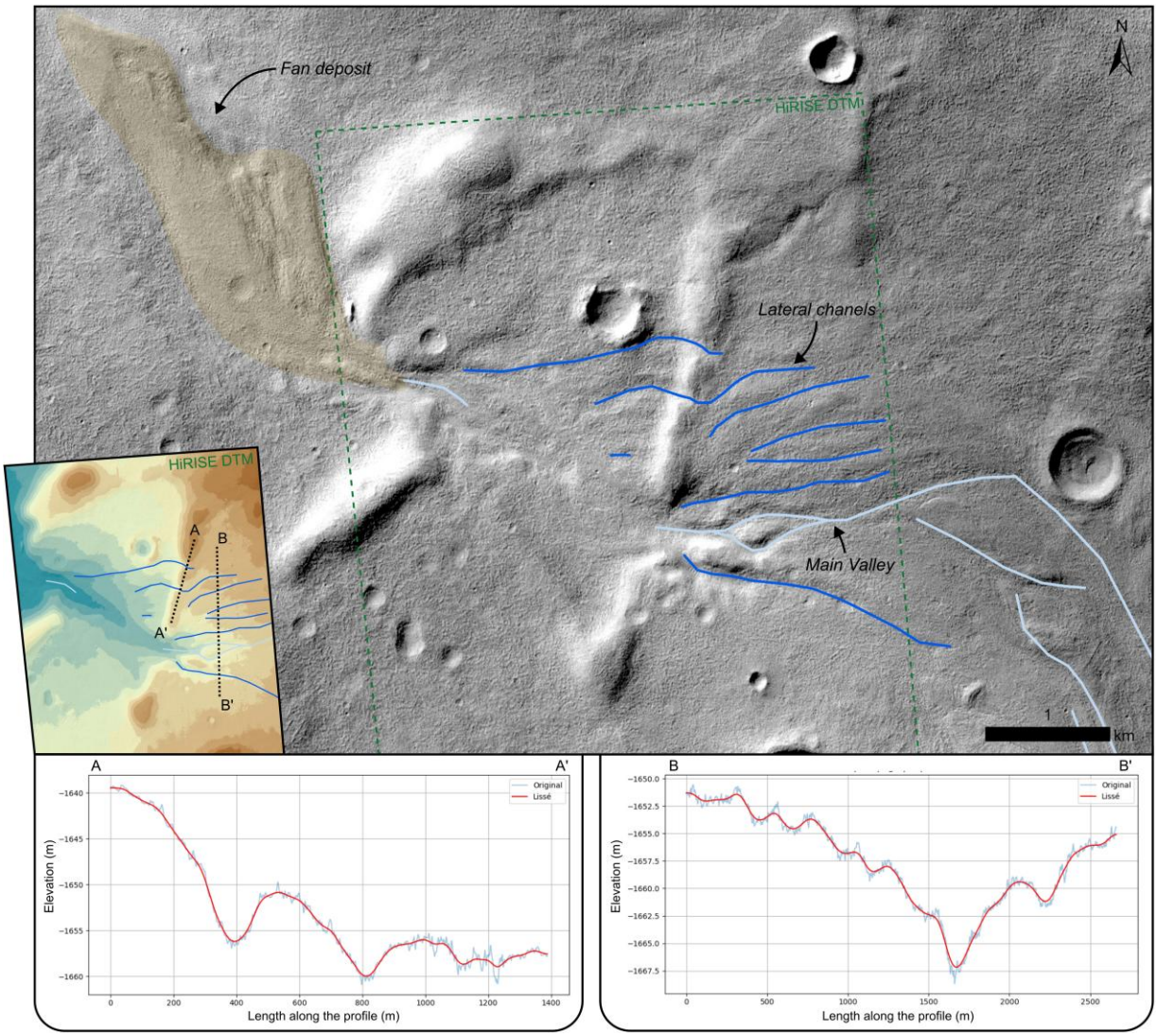

Figure 2: Case study: lateral channels and a main channel incising ridges and forming a fan-shaped structure at is terminus. Two panels show topographic profiles extracted from a HiRISE DTM generated using the stereo pair ESP_085542_1370 and ESP_085753_1370.

resolution of approximately 100 m/pixel[15]. This dataset permits also to better identify impact craters and their ejecta. Finally, we also find instances of ice deposits in our region of interest, including viscous flow features (VFFs) comprising concentric crater fills (CCF) and lobate debris aprons (LDA), as well as mantling deposits that increase in thickness and extent towards the south[3].

For a detailed analysis of valley segments, we used HiRISE imagery at resolutions of 25 cm/pixel and 1 m/pixel[15]. For this study, we extracted and produced HiRISE Digital Terrain Models (DTMs) from stereopairs at 1 m/pixel resolution, enabling a more detailed investigation of the structure and geometry of these landforms.

Topographic profiles were also extracted along the polylines of the selected valleys, which often extend over several hundred kilometers (beyond the coverage of HiRISE). For this purpose, we relied on PEDR point data from the Mars Orbiter Laser Altimeter (MOLA), which provides precise topographic measurements directly within the valley floors.

Finally, we used crater size-frequency distribution (CSFD) analysis, with the CraterStats software, to derive an absolute chronology. Craters were manually digitized on selected surfaces (mesas and basement) using ArcGIS software. Ages were estimated following the Hartmann & Daubar (2017) chronology system, applying differential, cumulative, and Poisson fitting methods[16]. We complemented this dataset with relative ages obtained by mapping cross-cutting relationships between the various landforms of interest.

Results:

The mapping (Fig. 1) reveals a geologically complex area where all landforms respond to the regional slope going toward the center of the Hellas. The relative chronology, based on cross-cutting relationships, identifies two generations of both ridges and wrinkle ridges, distinguished by their interactions with surrounding mesas: some ridges cut across the mesas, while others do not. Similarly, two generations of valleys are observed, with the younger valleys consistently incising the ridges. In some locations, evidence of viscous flow features (VFFs) and crater ejecta overlay the valleys, marking these as the most recent events in the region. Crater counting indicates ages of approximately 3.6 Ga for the mesas and 3.4 Ga for the basal unit. Additionally, this dating highlights a possible resurfacing event around 900 Ma. Based on relative chronology, there are two distinct valley formation events. The absolute chronology suggests that the studied landforms likely formed during these two periods, corresponding to the Late Hesperian and the Late Amazonian.

Understanding valley morphology is essential for reconstructing their formation processes. The mapping (Fig. 1) shows how the valleys incise into a gentle regional slope (less than −0.001%) trending toward the Hellas Basin. The valley system transitions from generally parallel valleys with a convergent drainage pattern -where sparse, relatively small tributaries flow into a main valley- to braided channels further west, downstream. This transition, highlighted by a green dotted line approximately along the eastern rim of the Apece crater, is further supported by topographic profiles extracted along the valley network.

Figure 2 presents a case study of a channel crossing two ridges, each approximately 300 to 600 m wide and predominantly oriented north-south. After incising the second ridge, the channel terminates in a fan-shaped deposit extending over 4 km downstream, reaching a maximum width of 1.4 km. No channels cut through this fan deposit.

The main valley is approximately 5 to 30 meters deep and 150 to 500 meters wide, bordered by channels forming a subparallel network on the valley sides, perched 7 to 15 meters above the valley floor, as shown in Fig. 2 (Profile B-B'). These channels are 5 to 10 meters deep and about 200 meters wide. They lack tributaries and join the main valley at oblique angles. Additionally, they do not appear to follow the local topographic gradient. Profile A-A' (Fig. 2) further reveals that some channels clearly cut across ridge crests, directly modifying and shaping the underlying relief.

Discussion and Conclusion:

The results suggest a high degree of complexity in the processes that have shaped the study area. According to the literature[6], this region belongs to the Hesperian and Noachian highlands, which aligns with our age estimates. An initial phase of erosive fluvial activity likely contributed to the formation of the mesas, with dating results suggesting an erosional period lasting around 200 million years.

Following this early phase, we propose a more recent episode of activity, dated to the Late Amazonian. Valleys intersect perpendicularly some of the ridges, suggesting a glacial assemblage. In this interpretation, ridges could correspond to moraines, while the associated valleys could be of sub-glacial origin. The precise distinction it still ongoing work.

Transition from convex to concave valley profiles observed in our study area may help define the location of a former glacial margin. However, these environments are complex and often reflect a palimpsest of glacial processes, where zones initially shaped subglacially may later evolve into proglacial settings. This could explain the heterogeneity observed in profiles, especially in the western part where it appears to be a point of curvature inflection system, while the Est area appear more convex.

Additionally, several channels flowing into the main valleys display morphologies consistent with lateral meltwater channels. On Earth, such features are typically interpreted as the interface between the glacier margin and the adjacent deglaciated terrain, marking

the transition between subglacial and proglacial environments. These channels commonly form along cold-based margins and are thought to be primarily fed by supraglacial meltwater.
These observations support the hypothesis of a glacial setting involving liquid water flow. This implies that liquid water may have existed on Mars during the Amazonian, likely in its earlier phase. To explain the presence of meltwater, we propose that volcanic activity in the upstream region may have triggered basal melting beneath an ice mass. Altogether, the geomorphological evidence points to two major flow episodes, with the most recent likely related to glacial activity involving liquid water, possibly indicating a previously unrecognized Amazonian glacial phase in the complex history of eastern Hellas.

References:

1. Forget, F., Haberle, R. M., Montmessin, F., Levrard, B., & Head, J. W. (2006). Formation of glaciers on Mars by atmospheric precipitation at high obliquity. Science, 311(5759), 368–371. https://doi.org/10.1126/science.1120335

2. Madeleine, J.-B., Forget, F., Head, J. W., Levrard, B., Montmessin, F., & Millour, E. (2009). Amazonian northern mid-latitude glaciation on Mars: A proposed climate scenario. Icarus, 203(2), 390–405. https://doi.org/10.1016/j.icarus.2009.04.037

3. Levy, J. S., Fassett, C. I., Head, J. W., Schwartz, C., & Watters, J. L. (2014). Sequestered glacial ice contribution to the global Martian water budget: Geometric constraints on the volume of remnant, midlatitude debris-covered glaciers. Journal of Geophysical Research: Planets, 119(10), 2188–2196. https://doi.org/10.1002/2014JE004685

4. Fastook, J. L., & Head, J. W. (2024). Modeling glaciation of the Hellas Basin, Mars, for a 'cold and icy' Late Noachian paleoclimatic scenario. Icarus, 421, 116222. https://doi.org/10.1016/j.icarus.2024.116222

5. Butcher, F. E. G. (2022). Water ice at mid-latitudes on Mars. In Oxford Research Encyclopedia of Planetary Science. Oxford University. https://doi.org/10.1093/acrefore/9780190647926.013.239

6. U.S. Geological Survey. (2014). Scientific Investigations Map.

7. Malin, M. C., Bell, J. F., Cantor, B. A., Caplinger, M. A., Calvin, W. M., Clancy, R. T., ... & Wolff, M. J. (2007). Context Camera Investigation on board the Mars Reconnaissance Orbiter. Journal of Geophysical Research: Planets, 112(E5). https://doi.org/10.1029/2006JE002808

8. Dickson, J. L., Pan, L., Edwards, C. S., McEwen, A. S., & Malin, M. C. (2024). The Global Context Camera (CTX) Mosaic of Mars: A product of information-preserving image data processing. Earth and Space Science, 11(7), e2024EA003555. https://doi.org/10.1029/2024EA003555

9. Christensen, P. R., Engle, E., Anwar, S., Dickenshied, S., Noss, D., Gorelick, N., & Weiss-Malik, M. (2009). JMARS - A Planetary GIS. AGU Fall Meeting Abstracts, IN22A-06. https://ui.adsabs.harvard.edu/abs/2009AGUFMIN22A..06C

10. Schultz, R. A. (2000). Localization of bedding plane slip and backthrust faults above blind thrust faults: Keys to wrinkle ridge structure. JGRP, 105(E5), 12035–12052.

11. Yin, A., & Wang, Y. (2023). Formation and modification of wrinkle ridges in the central Tharsis region of Mars as constrained by detailed geomorphological mapping and landsystem analysis. Earth and Planetary Physics, 7(2), 161–192.

12. Korteniemi, J., Raitala, J., Aittola, M., et al. (2010). Dike indicators in the Hadriaca Patera–Promethei Terra region, Mars. Earth and Planetary Science Letters, 294(3–4), 466–478. https://doi.org/10.1016/j.epsl.2009.06.038

13. Brož, P., Hauber, E., Platz, T., & Balme, M. (2015). Evidence for Amazonian highly viscous lavas in the southern highlands on Mars. Earth and Planetary Science Letters, 415, 200–212. https://doi.org/10.1016/j.epsl.2015.01.033

14. Farrand, W. H., Rice, J. W., Chuang, F. C., & Rogers, A. D. (2021). Spectral and geological analyses of domes in western Arcadia Planitia, Mars: Evidence for intrusive alkali-rich volcanism and ice-associated surface features. Icarus, 357, 114111. https://doi.org/10.1016/j.icarus.2020.114111

15. Fergason, R. L., Christensen, P. R., & Kieffer, H. H. (2006). High-resolution thermal inertia derived from the Thermal Emission Imaging System (THEMIS): Thermal model and applications. JGRP, 111(E12).

16. Hartmann, W. K., & Daubar, I. J. (2017). Martian cratering 11: Utilizing decameter scale crater populations to study Martian history. Meteoritics & Planetary Science, 52(3), 493–510. https://doi.org/10.1111/maps.12807